Available online at www.sciencedirect.com
ScienceDirect
Trans. Nonferrous Met. Soc. China 24(2014) 2904−2910
Transactions of Nonferrous Metals Society of China
www.tnmsc.cn

Effect of crystal orientation on tensile mechanical properties of single-crystal tungsten nanowire

Bin MA[1], Qiu-hua RAO[1], Yue-hui HE[2]

1. School of Civil Engineering, Central South University, Changsha 410075, China;
2. State Key Laboratory of Powder Metallurgy, Central South University, Changsha 410083, China

Received 4 March 2014; accepted 4 July 2014

Abstract: Based on the high-purity single-crystal tungsten nanowire firstly prepared by the metal-catalyzed vapor-phase reaction method, molecular dynamics method was used to calculate tensile stress−strain curves and simulate microscopic deformation structures of the single-crystal tungsten nanowires with different crystal orientations of ⟨100⟩, ⟨110⟩ and ⟨111⟩, in order to reveal the effect of crystal orientation on their tensile mechanical properties and failure mechanisms. Research results show that all of the stress−strain curves are classified into four stages: elastic stage, damage stage, yielding stage and failure stage, where ⟨100⟩ orientation has a special hardening stage after yielding and two descending stages. The crystal orientation has little effect on elastic modulus but great effect on tensile strength, yielding strength and ductility, depending on different atomic surface energies and principal sliding planes. The calculated values of elastic modulus are in good agreement with the tested values of elastic modulus.
Key words: crystal orientation; stress−strain curve; failure mechanism; molecular dynamics; single-crystal tungsten nanowire

1 Introduction

Single-crystal tungsten nanowire has excellent field-emission, optical, electrical and mechanical properties and wide application prospect as toughening-filling, photoelectric, structural materials [1,2]. Currently, it is prepared mainly by methods of high-temperature gas-phase deposition [3], electrochemical etching [4] and RF sputtering [5], where the growth process of tungsten nanowire cannot be better controlled. A new method of metal-catalyzed vapor-phase reaction has been firstly used to prepare the single-crystal tungsten nanowire (Fig. 1) [6] of high purity and complete body-centered cubic structure (BCC) by our research group [7,8]. As a new metal nanowire, its mechanical properties and failure mechanisms need to be further investigated.

Due to limitation in experimental conditions, computer simulation methods are usually adopted to study mechanical properties and failure mechanisms of metal nanowires including molecular dynamics simulation, Monte Carlo simulation and discreteness simulation methods, where the molecular dynamics method is widely applied [9]. Current literatures are mainly focused on the influencing factors of crystal orientation (important factor), structure size, temperature, loading rate for metal nanowires of face-centered cubic (FCC) structure, such as copper [10,11], aluminum [12,13], gold [14,15], and nickel [16,17]. However, there is short of systematic research on stress−strain curve and failure mechanism of the single-crystal tungsten nanowires with body-centred cubic (BCC) structure.

In this work, molecular dynamics method was used to study stress−strain curves and microscopic deformations of the single-crystal tungsten nanowires with different crystal orientations of ⟨100⟩, ⟨110⟩ and ⟨111⟩. Effects of crystal orientation on its mechanical properties and failure mechanisms were revealed in order to provide theoretical basis for optimal design and wide application of the single-crystal tungsten nanowire.

2 Calculation scheme

2.1 Calculation method

Large-scale atomic/molecular massively parallel simulator [18] (LAMMPS) based on the molecular dynamics method is adopted to simulate tensile mechanical behaviors of the single-crystal tungsten

Foundation item: Projects (50374082, 5071112018) supported by the National Natural Science Foundation of China
Corresponding author: Qiu-hua RAO; Tel: +86-13787265488; E-mail: raoqh@csu.edu.cn
DOI: 10.1016/S1003-6326(14)63425-7

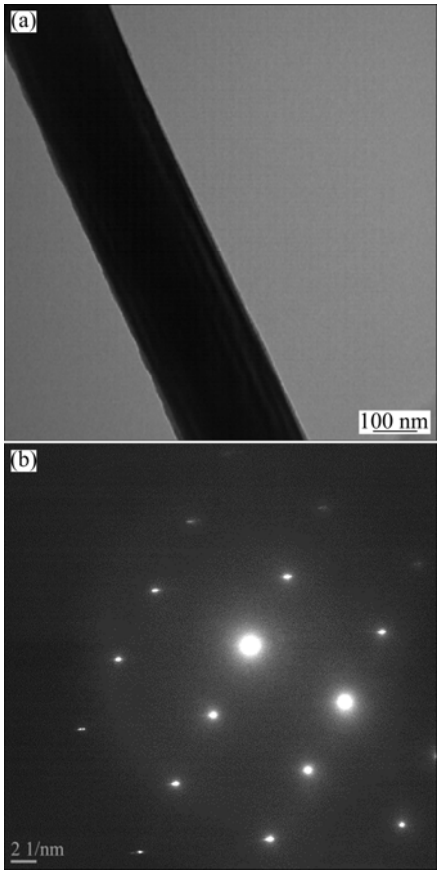

Fig. 1 SEM image (a) and electron diffraction pattern (b) of single-crystal tungsten nanowire [6]

nanowire. In nature, it is a particle method by calculating the space position of any particle based on the Newton second law as follows:

$$m_i\ddot{r}_i = -\nabla V \tag{1}$$

where m_i and $\ddot{r}_i$ are mass and space position of the particle i, respectively; V is potential energy function of the particle system; ∇ is spatial gradient [19].

Since the metal-atom interaction can be taken into account [20,21], embedded atom potential function is adopted and expressed as

$$V = \sum_i \left[\frac{1}{2} \sum_{j \neq i} \phi_{ij}(r_{ij}) + F(\rho_i) \right] \tag{2}$$

where $\phi_{ij}(r_{ij})$ is potential term, representing the interaction between atom i and j separated by a distance r_{ij}, and $F(\rho_i)$ is correction term, corresponding to embedded energy of the atom i embedding into the electron density $\rho(r_{ij})$. $\phi_{ij}(r_{ij})$, $F(\rho_i)$ and $\rho_i(r_{ij})$ are written as

$$\phi_{ij}\left(r_{ij}\right) = \frac{A\exp\left[-\alpha\left(r_{ij}/r_{\mathrm{e}}-1\right)\right]}{1+\left(r_{ij}/r_{\mathrm{e}}-\kappa\right)^{20}} - \frac{B\exp\left[-\beta\left(r_{ij}/r_{\mathrm{e}}-1\right)\right]}{1+\left(r_{ij}/r_{\mathrm{e}}-\lambda\right)^{20}} \tag{3}$$

$$F(\rho_i) = \begin{cases} \sum_{i=0}^{3} F_{ni}\left(\dfrac{\rho_i}{\rho_n}-1\right)^i, \rho_i < \rho_n, \rho_n = 0.85\rho_{\mathrm{e}} \\ \sum_{i=0}^{3} F_i\left(\dfrac{\rho_i}{\rho_{\mathrm{e}}}-1\right)^i, \rho_n \le \rho_i < \rho_0, \rho_0 = 1.15\rho_{\mathrm{e}} \\ F_{\mathrm{e}}\left[1-\ln\left(\dfrac{\rho_i}{\rho_{\mathrm{s}}}\right)^{\eta}\right]\left(\dfrac{\rho_i}{\rho_{\mathrm{s}}}\right)^{\eta}, \rho_0 \le \rho_i \end{cases} \tag{4}$$

$$\rho_i(r_{ij}) = \sum_{j, j\neq i} f_j\left(r_{ij}\right) \tag{5}$$

where r_{e} is the equilibrium spacing between the nearest neighbors; A, B, α and β are four adjustable parameters; κ and λ are two additional parameters for the cutoff; $f_j\left(r_{ij}\right)$ is the electron density at the site of atom i arising from atom j at a distance r_{ij} away and is expressed as

$$f_j\left(r_{ij}\right) = \frac{f_{\mathrm{e}}\exp\left[-\beta\left(r_{ij}/r_{\mathrm{e}}-1\right)\right]}{1+\left(r_{ij}/r_{\mathrm{e}}-\lambda\right)^{20}} \tag{6}$$

The electron density function is taken the same form as the attractive term in the pair potential with the values of β and λ.

2.2 Calculation model

As shown in Fig. 2, the single-crystal tungsten nanowire was square with dimensions of 25.28 nm× 2.528 nm× 2.528 nm and initial lattice constant of 0.316 nm. The initial configuration of ⟨100⟩ crystal orientation was ideal lattice of BCC structure and its coordinate axes of x, y, z were in the [100], [010], [001] crystal orientations, respectively. The initial configurations of ⟨110⟩ and ⟨111⟩ crystal orientations were obtained by rotating the ideal lattice of BCC structure to keep the crystal orientations of [110] and [111] parallel to x axis. Boundary conditions were periodic boundary in x direction and free boundary in y and z directions. In the

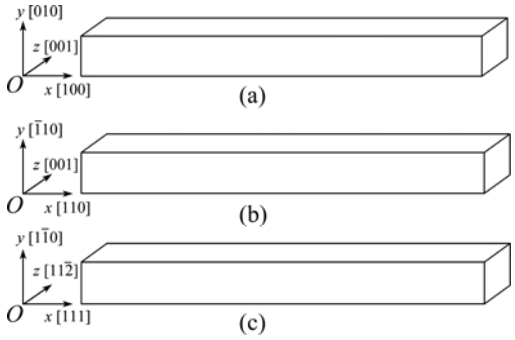

Fig. 2 Initial configurations of single-crystal tungsten nanowires with different crystal orientations: (a) ⟨100⟩ crystal orientation; (b) ⟨110⟩ crystal orientation; (c) ⟨111⟩ crystal orientation

relaxing process of the initial configuration, temperature was 1 K under isothermal−isobaric condition, time step was 0.002 ps and relaxation time was 200 ps in order to ensure full relaxation of the initial configurations nearly to equilibrium state.

Figure 3 shows the initial microstructures of the single-crystal tungsten nanowires with different crystal orientations after full relaxation. It is seen that the surface atoms of ⟨100⟩ crystal orientation are in ideal lattice array. The surface atoms of ⟨110⟩ crystal orientation are in square grid array of *xz* plane and in diamond grid array of *xy* plane, while the surface atoms of ⟨111⟩ crystal orientation are in square grid array of *xz* and *xy* planes. Table 1 lists surface atom distances of the single-crystal tungsten nanowires with different crystal orientations along *x*, *y*, *z* directions. Obviously, different crystal orientations result in different lattice arrangements and surface atom structures.

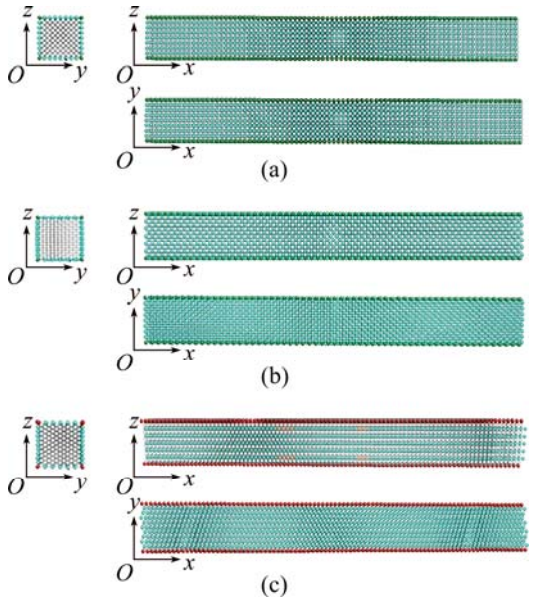

Fig. 3 Initial microstructures of single-crystal tungsten nanowires with different crystal orientations: (a) ⟨100⟩ crystal orientation; (b) ⟨110⟩ crystal orientation; (c) ⟨111⟩ crystal orientation

Table 1 Surface atom distances of single-crystal tungsten nanowires with different crystal orientations along *x*, *y* and *z* directions

Crystal orientation	L_x/nm	L_y/nm	L_z/nm
⟨100⟩	0.316	0.316	0.316
⟨110⟩	0.447	0.447	0.316
⟨111⟩	0.548	0.447	0.516

In simulating calculation, the initial microstructures were subjected to quasi-static tensile loading in *x*-axis direction under displacement control step by step until failure. At each step the tensile strain was 0.004 and the relaxation time was 10 ps, enough for full relaxation until reaching equilibrium.

3 Simulation results and analyses

Figure 4 shows stress−strain curves of the single-crystal tungsten nanowires with different crystal orientations, which can be divided into four stages: *OA* (*OA*$_1$, *OA*$_2$, *OA*$_3$), *AB*(*A*$_1$*B*$_1$, *A*$_2$*B*$_2$, *A*$_3$*B*$_3$), *BC*(*B*$_1$*C*$_1$, *B*$_2$*C*$_2$, *B*$_3$*C*$_3$), *CD*(*C*$_1$*D*$_1$, *C*$_2$*D*$_2$, *C*$_3$*D*$_3$), with additional stage (*C*$_1$*E*$_1$) specially for ⟨100⟩ crystal orientation.

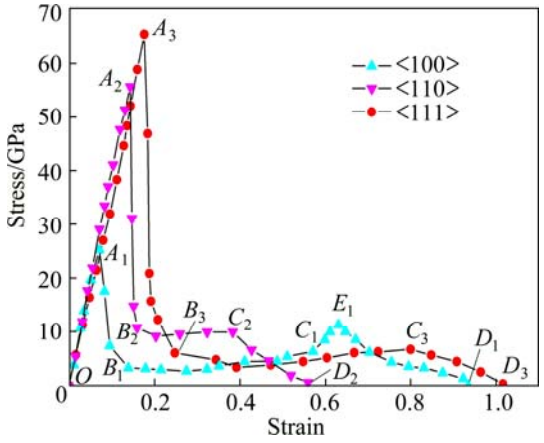

Fig. 4 Stress−strain curves of single-crystal tungsten nanowires with different crystal orientations

3.1 Elastic stage (*OA*)

In *OA* stage, the stresses of the single-crystal tungsten nanowires with different crystal orientations are all linearly increased with increasing the strains (i.e., elastic stage). Figure 5 shows microstructures of the single-crystal tungsten nanowires with different crystal orientations (any point of *OA* stage), where all lattices are complete and atomic arrays are regular. Elastic modulus of the single-crystal tungsten nanowires with ⟨100⟩, ⟨110⟩ and ⟨111⟩ crystal orientations can be obtained by numerical fitting of the *OA* linear segment. They are 375, 397 and 368 GPa, respectively, which are

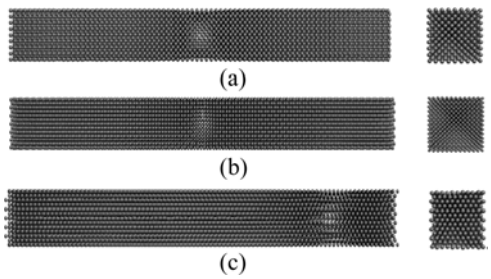

Fig. 5 Microstructures of single-crystal tungsten nanowires with different crystal orientations (any point of *OA* stage): (a) ⟨100⟩ crystal orientation (ε=5.6%); (b) ⟨110⟩ crystal orientation (ε=8.0%); (c) ⟨111⟩ crystal orientation (ε=12.4%)

in good agreement with the range of elastic modulus measured by bending test [22] and nano-indentation test [8].

It is also found that tensile strengths of the single-crystal tungsten nanowires with ⟨100⟩, ⟨110⟩ and ⟨111⟩ crystal orientations are 25.4, 55.8 and 66.7 GPa, which are mainly affected by surface energy. Since ⟨111⟩ crystal orientation has the maximum surface-atom distance (Table 1) and the minimum surface-atom density under the same size, it has the lowest surface energy and the most stable atom structure, which results in the strongest ability of resisting failure and the maximum tensile strength. This result is consistent with that in Ref. [23].

3.2 Damage stage (*AB*)

In *AB* stage, the stresses of the single-crystal tungsten nanowires with different crystal orientations are all decreased with increasing strains. Figure 6 shows microstructures of the single-crystal tungsten nanowires with different crystal orientations (any point in *AB* stage), where most of the atomic lattice structures are still in regular array of BCC structures but with different local deformations. For the ⟨100⟩ crystal orientation, twin bands with some irregular FCC structures (Figs. 6(a) and (b)) appear because of local atomic layers slipping on the {110} surface. For the ⟨110⟩ crystal orientation, local atomic dislocations result in twin bands with some regular FCC structures (Figs. 6(c) and (d)). For the ⟨111⟩ crystal orientation, local atomic stacking caused by local atomic layers slipping on the {112} surface would lead to some HCP structures (Figs. 6(e) and (f)). The irreversible deformation of atomic dislocation results in decrease of loading capacity and thus *AB* stage is named as damage stage [24].

3.3 Yielding stage (*BC*)

In *BC* stage, the stresses of the single-crystal tungsten nanowires with different crystal orientations are slightly fluctuated but the strains are increased greatly (i.e., yielding stage). Figure 7 shows microstructures of the single-crystal tungsten nanowires with different crystal orientations (point *C*). For the ⟨100⟩ crystal orientation (Figs. 7(a) and (b)), the twin bands occur in *AB* stage and gradually extend to cover the whole nanowire, which results in relatively regular atomic array and diamond cross-section changing from its initial square configuration (i.e., transition). For the ⟨110⟩ crystal orientation (Figs. 7(c) and (d)), the serious atomic dislocations lead to damage of its lattice structure (irregular cross-section) and cause the atomic collapse and necking areas. Although the ⟨111⟩ crystal orientation is still in regular atomic array but its cross-section is

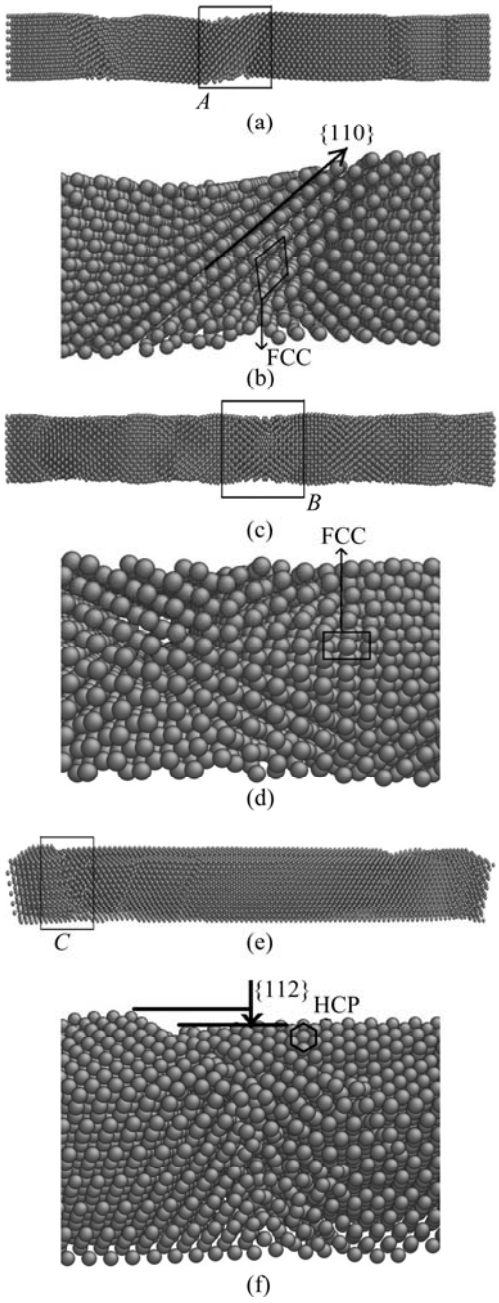

Fig. 6 Microstructures of single-crystal tungsten nanowires with different crystal orientations (any point of *AB* segment): (a) ⟨100⟩ crystal orientation (ε=10.4%); (b) Enlargement of region *A*; (c) ⟨110⟩ crystal orientation (ε=16.0%); (d) Enlargement of region *B*; (e) ⟨111⟩ crystal orientation (ε=20.4%); (f) Enlargement of region *C*

changed from the initial square to rectangle with incomplete lattice structure caused by a lot of atomic defects (Figs. 7(e) and (f)).

It is also found that yield strengths of the single-crystal tungsten nanowires with ⟨100⟩, ⟨110⟩ and ⟨111⟩ crystal orientations are 3.3, 9.3 and 5.6 GPa, respectively. Since the primary slip plane of BCC-structural metal nanowire is {110} surface [25,26] and it only exists in

the ⟨111⟩ and ⟨100⟩ crystal orientations under tensile loading, the ⟨111⟩ and ⟨100⟩ crystal orientations could easily yield and have lower yield strength than the ⟨110⟩ crystal orientation.

3.4 Hardening stage (C_1E_1)

As shown in Fig. 4, the single-crystal tungsten nanowire with ⟨100⟩ crystal orientation is excepted. Its stress is increased with increasing strain once again after the yielding stage in C_1E_1 segment (i.e., hardening stage [24]), since only the ⟨100⟩ crystal orientation has phase transition in *BC* stage and can recover its loading capacity.

Comparison of the stress values of the point A_1 and point E_1 shows that the maximum stress in hardening stage is much smaller than its tensile strength because the stress of C_1E_1 segment is hardened only based on yielding stage (*BC* segment).

3.5 Failure stage (E_1D_1, C_2D_2, C_3D_3)

In E_1D_1, C_2D_2, C_3D_3 stages, the stresses of the single-crystal tungsten nanowires with different crystal orientations are all decreased to zero as the strains are increased (i.e., failure stage). Figure 8 shows the microstructures of the single-crystal tungsten nanowires with different crystal orientations, where there are necking zones appearing and developing to failure but the forming mechanisms of necking zones are different

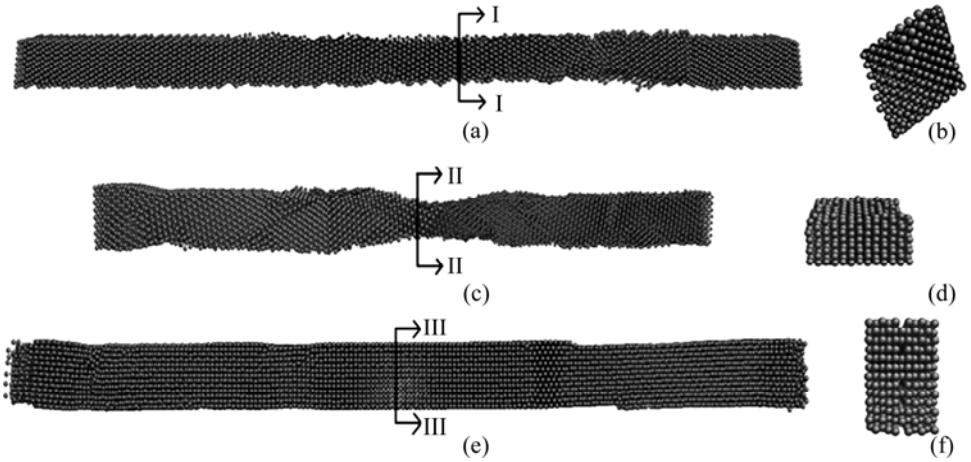

Fig. 7 Microstructures of single-crystal tungsten nanowires with different crystal orientations (point *C*): (a) ⟨100⟩ crystal orientation (ε=58.4%); (b) Enlargement of section I−I; (c) ⟨110⟩ crystal orientation (ε=32.0%); (d) Enlargement of section II−II; (e) ⟨111⟩ crystal orientation (ε=68.4%); (f) Enlargement of section III−III

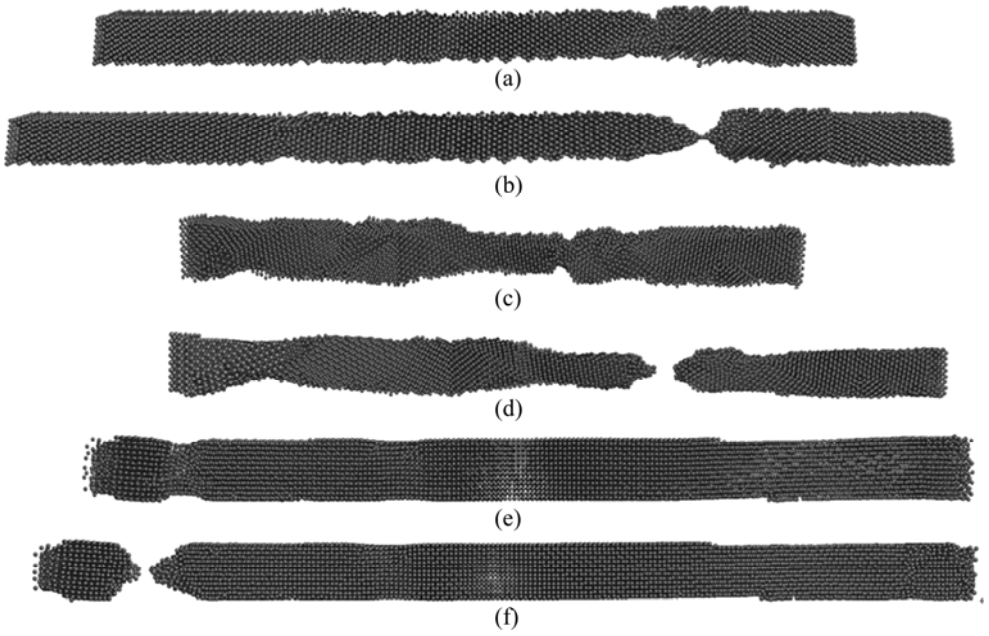

Fig. 8 Microstructures of single-crystal tungsten nanowires with different crystal orientations (E_1D_1, C_2D_2, C_3D_3 segments): (a) ⟨100⟩ crystal orientation (point E_1, ε=64.0%); (b) ⟨100⟩ crystal orientation (point D_1, ε=93.2%); (c) ⟨110⟩ crystal orientation (point C_2, ε=36.0%); (d) ⟨110⟩ crystal orientation (point D_2, ε=56.0%); (e) ⟨111⟩ crystal orientation (point C_3, ε=74.0%); (f) ⟨111⟩ crystal orientation (point D_3, ε=101.6%)

in different crystal orientations.

For the ⟨100⟩ crystal orientation (Figs. 8(a) and (b)), most of atoms are regularly arranged but local atomic lattice structures are completely destroyed by dislocation, which leads to irregular twin bands, sharp notches and final necking zones, gradually. For the ⟨110⟩ crystal orientation (Figs. 8(c) and (d)), most of atoms are irregularly arranged and local atomic dislocations result in atomic stacking, sharp notches and final necking region. Obviously, most of atoms are also regularly arranged in the ⟨111⟩ crystal orientation (Fig. 8(e)) but local atomic dislocations cause atomic stacking and final necking regions without sharp notch (Fig. 8(f)).

By comparing the strain values of points D_1, D_2 and D_3, it is found that the total strains of the ⟨100⟩, ⟨110⟩, ⟨111⟩ crystal orientations are 93.2%, 56% and 101.6%, indicating that the ⟨100⟩ and ⟨111⟩ crystal orientations are strong ductile materials while the ⟨110⟩ crystal orientation is weak ductile material. Clearly, the total strains depend mainly on the yielding-stage strains, as shown in Fig. 4. Since three crystal orientations except the ⟨110⟩ crystal orientation have the primary slip planes of {110} surface under tensile loading, the ⟨100⟩ and ⟨111⟩ crystal orientations could easily deform in plasticity and thus their plastic strains are larger than that of the ⟨110⟩ crystal.

4 Conclusions

1) Stress−strain curves of the single-crystal tungsten nanowires with different orientations can be classified into four stages: elastic stage, damage stage, yield stage and failure stage, where the ⟨100⟩ orientation has a special hardening stage after yielding and two descending stages since it can recover carrying capacity after the phase transition in the yield stage. The first stress drop is caused by irreversible change of the local atomic dislocation and twinning, and the second stress drop is due to the lattice structure failure which leads to final fracture of material.

2) Calculated results of elastic modulus are in good agreement with test results of elastic modulus of the single-crystal tungsten nanowires. The crystal orientation has little effect on the elastic modulus but great effect on the tensile strength, which is mainly affected by surface energy. The ⟨111⟩ crystal orientation has the smallest surface energy and thus the largest tensile strength.

3) The crystal orientation has great effect on yield strength and total strain, depending on whether there is primary slip plane or not. Since the primary slip plane of BCC-structural metal nanowire is {110} surface existing only in the ⟨111⟩ and ⟨100⟩ crystal orientations, the ⟨110⟩ crystal orientation without the primary slip plane has the smallest yield strength and yielding-stage strain. The ⟨110⟩ crystal orientation of single-crystal tungsten nanowire is weak ductile material while the ⟨100⟩ and ⟨111⟩ crystal orientations of single-crystal tungsten nanowire are strong ductile materials.

References

[1] MA Yun-zhu, SHI Yu-bin, LIU Wen-sheng. Structure characterization and properties research of tungsten whiskers/nanaowires [J]. Materials Review, 2012, 26(2): 25−29. (in Chinese)

[2] KIM J C, RYU S S, LEE H. Metal injection molding of nanostructured W−Cu composite powder [J]. The Inter J of Powder Metall, 1999, 35(4): 47−55.

[3] SREERAM V, HARI C, MAHENDRA K S. Vapor phase synthesis of tungsten nanowires [J]. J Amchem Soc, 2003, 125(36): 10792−10793.

[4] OLIVIER L G, JOACHIM W A, MOON C J, PETER C G, JOHN T Y. Reproducible electrochemical etching of tungsten probe tips [J]. Nano Lett, 2002, 2(3): 191−193.

[5] TANSEL K, WANG P I, WANG G C, LU T M. Phase transformation of single crystal β-tungsten nanorods at elevated temperatures [J]. Thin Solid Films, 2005, 493(2): 293−296.

[6] WANG S L, HE Y H, ZOU J, JIANG Y, XU J, HUANG B Y, LIU C T, LIAW P K. Synthesis of single-crystalline tungsten nanowires by nickel-catalyzed vapor-phase method at 850 °C [J]. Journal of Crystal Growth, 2007, 306(2): 433−436.

[7] WANG S L, HE Y H, FANG X S, ZOU J, WANG Y, HUANG H, COSTA P M F J, SONG M, HUANG B Y, LIU C T, LIAW P K, BANDO Y, GOLBER G. Structure and field-emission properties of sub-micrometer-sized tungsten-whisker arrays fabricated by vapor deposition [J]. Advanced Materials, 2009, 21(23): 2387−2392.

[8] HUANG H, WU Y Q, WANG S L, HE Y H, ZOU J, HUANG B Y, LIU C T. Mechanical properties of single crystal tungsten microwhiskers characterized by nanoindentation [J]. Materials Science and Engineering A, 2009, 523(2): 193−198.

[9] WU Heng-an, WANG Xiu-xi, NI Xiang-gui. Direct atomistic computing on the elastic modulus of metal nanorod [J]. Acta Metall Sin, 2002, 38(11): 1219−1222. (in Chinese)

[10] WANG D X, ZHAO J W, HU S, YIN X, LIANG S, LIU Y H, DENG S Y. Where, and how, does a nanowire break? [J]. Nanoletters, 2007, 7(5): 1208−1212.

[11] CAO A, MA E. Sample shape and temperature strongly influence the yield strength metallic nanopillars [J]. Acta Materialia, 2008, 56(17): 4816−4828.

[12] HUANG Dan, TAO Wei-ming, GUO Yi-mu. Molecular dynamics simulation of failure process of nano aluminum wire under axial tension [J]. Ordnance Material Science and Engineering , 2005, 28(3): 1−3. (in Chinese)

[13] WARD D K, CURTIN W A, YUE Q. Aluminum−silicon interfaces and nanocomposites: A molecular dynamics study [J]. Composites Science and Technology, 2006, 66(9): 1151−1161.

[14] CHEN D L, CHEN T C. Mechanical properties of Au nanowires under uniaxial tension with high strain-rate by molecular dynamics [J]. Nanotechnology, 2005, 16(12): 2972−2981.

[15] PARK H S, ZIMMERMAN J A. Modeling inelasticity and failure in gold nanowires [J]. Physical Review B, 2005, 72(5): 054106−054115.

[16] WEN Y H, ZHU Z Z, ZHU R Z. Molecular dynamics study of the mechanical behavior of nickel [J]. Computational Materials Science, 2007, 41(4): 553−560.

[17] HUANG Dan, GUO Yi-mu. Mechanical behavior and properties of three kinds of nano-scale materials made of monocrystalline nickel [J]. The Chinese Journal of Nonferrous Metals, 2006, 16(8):

1368−1373. (in Chinese)
[18] PLIMPTON S. Fast parallel algorithms for short-range molecular dynamics [J]. Journal of Computational Physics, 1995, 117(1): 1−19.
[19] LI Ming-lin, LIN Fan, CHEN Yue. Study on the mechanical properties of carbon nanocones using molecular dynamics simulation [J]. Acta Phys Sin, 2013, 62(1): 016102-1. (in Chiness)
[20] FOILES S M, BASKES M I, DAW M S. Embedded-atom-method functions for the fcc metals Cu, Ag, Au, Ni, Pd, Pt, and their alloys [J]. Physical Review B, 1986, 33(12): 7983−7991.
[21] ZHOU X W, JOHNSON R A, WADLEY H N G. Misfit –energy-increasing dislocations in vapor-deposited CoFe/NiFe multilayers [J]. Physical Review B, 2004, 69: 144113-1−10.
[22] VOLKER C，CLAUS C R，JORG P, MERTEN N, OLIVER A, KLEMENSl B, MATTHIAS H, JOCHEN W, SRDJAN M, ANDREW J S, ACHIM W H. Nanomechanics of single crystalline tungsten nanowires [J]. Journal of Nanomaterials, 2008, 2008: 638947-1−9.
[23] LU Hong-quan, ZHANG Jun-qian, FAN Jing-hong. Molecular dynamics study of the tensile mechanical behavior of metallic nanowires with different orientation [J]. Chinese Journal of Solid Mechanics, 2011, 32(5): 433−439. (in Chinese)
[24] MA Bin, RAO Qiu-hua, HE Yue-hui, WANG Shi-liang. Molecular dynamics simulation of tensile deformation mechanism of the single crystal tungsten nanowire [J]. Acta Phys Sin, 2013, 17(62): 176103-1. (in Chinese)
[25] CHRISTIAN J W. Some surprising features of the plastic deformation of body-centered cubic metals and alloys [J]. Metall Trans A, 1983, 14(7): 1237−1256.
[26] JIN Hui-qiang, WANG You-liang, AN Chang-xing. Determination of the choice of slip systems for bcc metals by molecular orbital theory [J]. Journal of Shenyang Institute of Technology, 1998, 17(3): 20−24. (in Chinese)

晶向对单晶钨纳米线拉伸力学性能的影响

马 彬[1]，饶秋华[1]，贺跃辉[2]

1. 中南大学 土木工程学院，长沙 410075；
2. 中南大学 粉末冶金国家重点实验室，长沙 410083

摘 要：采用金属催化的气相合成法制备高纯度单晶钨纳米线材料，采用分子动力学方法进行拉伸模拟计算，分析⟨100⟩、⟨110⟩、⟨111⟩ 3 种典型晶向下单晶钨纳米线的拉伸应力−应变曲线及其微观变形结构，揭示晶向对单晶钨纳米线拉伸破坏机理的影响。结果表明：3 种晶向均具有弹性、损伤、屈服、破坏等 4 个阶段，其中⟨100⟩晶向还具有独特的屈服后强化阶段和两次应力突降阶段。晶向对单晶钨纳米线弹性模量的影响较小，对抗拉强度、屈服强度和延展性的影响较大，主要取决于不同的原子表面能和主滑移面。计算得到的单晶钨纳米线的弹性模量值与实测结果吻合较好。

关键词：晶向；应力−应变曲线；破坏机理；分子动力学；单晶钨纳米线

(Edited by Xiang-qun LI)